Field-Induced Partial Disorder in a Shastry-Sutherland Lattice

Madalynn Marshall[1], Brianna R. Billingsley[2], Xiaojian Bai[1], Qianli Ma[1], Tai Kong[2,3], Huibo Cao[1*]

[1]*Neutron Scattering Division, Oak Ridge National Laboratory, Oak Ridge, Tennessee 37831, USA*

[2]*Department of Physics, University of Arizona, Tucson, Arizona, 85721*

[3]*Department of Chemistry and Biochemistry, University of Arizona, Tucson, Arizona, 85721*

**email:* caoh@ornl.gov

Abstract

The Shastry-Sutherland lattice (SSL), a 2-dimensional orthogonal arrangement of the spin dimers, has been realized in $BaNd_2ZnS_5$. Single crystal neutron diffraction reveals a 2-Q antiferromagnetic order of the ferromagnetic dimers below T_N = 2.9 K. This magnetic order can be understood by the orthogonal arrangement of local Ising Nd spins that was identified by the local magnetic susceptibility method through polarized neutron diffraction. A field was applied along [1 -1 0] to probe the observed metamagnetic transition in the magnetization measurement. Each propagation vector of 2-Q magnetic order corresponds to one of the two magnetic sublattices by considering the centering translation of the body centered symmetry. Each sublattice shows a "stripe" order with a Neél-type arrangement in each single layer. The "stripe" order with $\mathbf{q_1}$= (½, ½, 0) remains nearly intact up to 6 T, while the other one with $\mathbf{q_2}$ = (-½, ½, 0) is suppressed at ~1.7 T, indicating that a partially disordered, liquid-like state of ferromagnetic dimers forms at the critical field H_c=1.7 T. The H_c varies with temperature and is manifested in the *H*-*T* phase diagram constructed by measuring the magnetization in $BaNd_2ZnS_5$. Above the H_c, a critical region, the liquid state of ferromagnetic dimers, exists before the full polarized dimer phase.

Introduction

Exotic non-trivial magnetic behavior has emerged in magnetic systems with geometrical frustration. The kagomé and triangular lattices are common examples of two-dimensional (2D) frustrated lattices.[1,2] More elusive is the 2D orthogonal dimer lattice famously realized in the material $SrCu_2(BO_3)_2$[3,4], which has been discovered to host a quantum spin liquid phase [5–8]. This lattice can be described by the Shastry-Sutherland (SS) model which consists of a 2D orthogonal arrangement of the spin dimers where the ratio between the two magnetic interactions, $\delta = J_1/J_2$ with J_1 and J_2 as the antiferromagnetic intra- and inter-dimer interactions, respectively, is critical for understanding the magnetic behavior with the Shastry-Sutherland lattice (SSL).[9] The δ ratio of 0.675 and 0.765 separate the dimer singlet, plaquette singlet and Neél phase, respectively, in the phase diagram of the SS model.[10,11]

Resultantly, rich magnetic phase diagrams have been constructed for SSL materials from the field-induced evolution of the magnetic order. One common feature are fractionalized magnetization plateaus, which may originate from the transition of a dimer singlet ground state to the formation of ordered superstructures of the localized field-induced triplet dimers such as in $SrCu_2(BO_3)_2$.[10,12–21] The SSL is also found in families such as the rare earth tetraborides RB_4 (R=rare earth)[22–24], BaR_2TO_5 (R=rare earth, T=transition metal)[25–28], R_2T_2In (R=rare earth, T=transition metal)[29–31] and RE_2Pt_2Pb (R=rare earth)[32]. The magnetic ordered states can vary significantly from the insulator $SrCu_2(BO_3)_2$ which possesses a Heisenberg type exchange interaction to the metallic RB_4 family where a Ruderman-Kittel Kasuya-Yosida (RKKY) type interaction is observed between the moments giving it a long-rang order and possessing Ising-like moments oriented perpendicular to the SSL planes.[33–35] However, SSL materials such as Yb_2Pt_2Pb

[32,36–39], have been found to exhibit field-induced metamagnetic transitions associated with partially disordered states, where at low temperatures a Luttinger liquid state has been realized.[40]

Consequently, only very few SSL materials were reported to possess ferromagnetic dimers, including the insulator $BaNd_2ZnO_5$[25] and metallic TmB_4[23,34,41]. Considering the newly explored BaR_2TO_5 family, although it is chemically diverse the formation of the SSL will only occur for the lighter rare earth elements and successful single crystal growth has not been reported. The sulfide counterpart, BaR_2TS_5, which crystallizes into the same space group (*I*4/*mcm*) as the SSL BaR_2TO_5 materials, remains largely unexplored and recently large single crystals of $BaNd_2ZnS_5$[42] have been synthesized exhibiting a T_N = 2.9 K. The dimers of the SSL in $BaNd_2ZnS_5$ are formed by the Nd atoms having inter-dimer lengths of 4.151 Å and intra-dimer lengths of 3.596 Å. A metamagnetic transition is observed in the $M(H)$ with **H** along [1 -1 0], indicating this SSL material an excellent model for studying the intricate dimer physics from the field-induced phase evolution of SSL materials. Here we utilize polarized neutrons to provide insight into the local magnetic anisotropy of Nd spins and reveal the cause of 2-Q magnetic order. The resulting field-induced evolution of the magnetic phases were characterized by magnetization measurements with the critical input from single crystal neutron diffraction. A partial disordered liquid-like state of dimers was found and a "spin-flip-or-flop" mechanism was proposed to describe the liquid state of ferromagnetic dimers.

Results and discussions

Zero field Magnetic Structure Determination.

$BaNd_2ZnS_2$ exhibits 2D SSL layers of magnetic Nd atoms separated by layers of Ba and Zn atoms and coordinated by S atoms. Figure 1*a*, describes the Nd SSL where J_1 represents the intradimer interaction (nearest-neighbor) and J' the interdimer interaction (next-nearest-neighbor), a typical SS interaction model. To understand the magnetic anisotropy of the Nd spins in $BaNd_2ZnS_5$, we measured the local magnetic susceptibility tensor of the Nd spins by polarized neutron diffraction.[43,44] The local symmetry of the Nd atomic site, the 8*h* site of space group *I*4/*mcm*, implies the principal axes of the ellipsoid are along the [1 1 0], [1 -1 0] and [0 0 1] directions. The bulk magnetic measurements have revealed the magnetic moments are easy in-plane.[45] Therefore, only one-field-direction along [1 -1 0], was selected to detect the in-plane magnetic anisotropy of the Nd spins. By measuring reflections in spin-up and spin-down neutron channels, we obtained 17 good-quality flipping ratios to refine two free susceptibility tensor parameters in-plane. A suitable fitting of the flipping ratios could be reached, as shown by the Figure 1*b* plot of the experimental versus calculated flipping ratios, using the software CrysPy. The in-plane principal axes of the Nd magnetization ellipsoids, Figure 1*c*, were found to be orthogonal to the dimer bond consistent with an Ising-spin nature with lengths $\chi_{//} = 0.221(36)\ \mu_B/T$ and $\chi_{\perp} = 0.049(36)\ \mu_B/T$. Similar to Yb_2Pt_2Pb[32] the magnetic moments are found within the plane of the SSL and orthogonally arranged between two magnetic sublattices that satisfy the Ising behavior, contrary to that in $SrCu_2(BO_3)_2$[14] and TmB_4[23]. Instead of the well-known SSL interaction model, the resulting formation seemingly favors an effective square lattice magnetic model where J_1 and J_2 are the potential interaction paths, as indicated by the orange line (i.e. the dimer bond) and the dashed black line, respectively, in Figure 1*f*.[32] The orthogonal spin arrangement between

the neighboring orthogonal dimer bonds suppresses the major symmetric interactions. While the asymmetric terms are likely weak as well, this will be shown by the field measurements presented later. We can likely conclude that the interdimer interaction J' is minimal. Future inelastic neutron scattering measurements are necessary to further confirm the speculation here and interpret the spin dynamics in $BaNd_2ZnS_5$.

From the temperature-dependence of the magnetic scattering at (½ ½ 2), Figure 1*d*, the magnetic order appears at ~ 3 K, consistent with the reported T_N = 2.9 K from the magnetic susceptibility measurements.[45] The solid red line in Figure 1*d*, corresponds to the power law fitting of the intensity, $I = A(T_N - T/T_N)^{2\beta} + B$, with a T_N reasonably fixed at 2.95 K, A ~ 33710, B ~ -14315 and a $\beta \sim 0.08(1)$ which is smaller than the expected $\beta = 1/8$ for a 2D Ising system[32] and might be a result from the nature of spin dimer lattice. As a product of the single crystal polarized neutron diffraction results, a suitable magnetic structure model could be immediately determined and the fit could be appropriately constrained with moments perpendicular to the dimer bonds. A 2-**Q** AFM model consisting of two magnetic sublattices indexed by the propagation vectors $\mathbf{q_1}$= (½, ½, 0) and $\mathbf{q_2}$= (-½, ½, 0), resembling the AFM 2-**Q** structure for $BaNd_2ZnO_5$[25], best fit the zero-field data. The magnetic symmetry *P_C*4/*nnc* (#126.385) was then determined using the k-SUBGROUPSMAG program from the Bilbao Crystallographic server. Based on the body centered symmetry, the SSL layers are separated by a centering translation resulting in two inequivalent propagation vectors that each connects to one magnetic sublattice with a "stripe" order when viewing two layers together. Therefore, an interlayer interaction, J_z, should also be considered, where the nearest interlayer neighbor is likely a FM interaction to result in the magnetic order at zero field. Each SSL layer individually exhibits a Neél phase arrangement where the potential interaction paths consist of FM J_1 and AFM J_2. The refined Nd magnetic moment was determined

to be 2.6(1) μ_B. Figure 1*e* shows a plot of the calculated structure factor square (F^2_{calc}) versus the observed one (F^2_{obs}) and the magnetic structure can be seen in Figure 1*f* where the orange and blue atoms represent the two different sublattices and the overlapping layers along the *c* axis are indicated by the light and dark color shades.

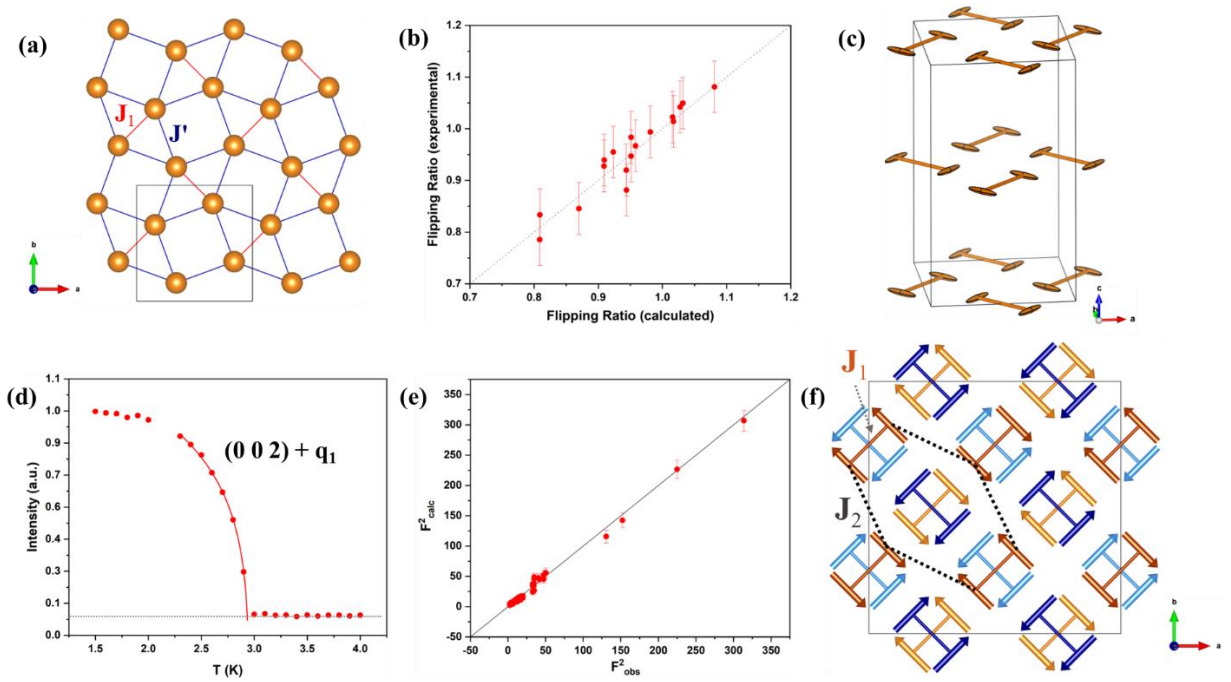

Figure 1. a SSL sublattice of Nd atoms in the *ab* plane**. b** Experimental versus calculated flipping ratio plot. **c** Local magnetic anisotropy of Nd dimers is showed by magnetic susceptibility tensors drew as ellipsoids in unit cell of $BaNd_2ZnS_5$. **d** Temperature-dependent order parameter of peak (½ ½ 2), red line is the empirical power law fitting, $I = A(T_m - T/T_m)^{2\beta} + B$. **e** Experimental versus calculated structure factors at zero field. **f** 2-**Q** magnetic structure model for $BaNd_2ZnS_5$, the blue and orange represent the sublattices with $\mathbf{q_1}$= (½, ½, 0) and $\mathbf{q_2}$= (-½, ½, 0), respectively, and the light and dark color shades represent the different layers along the *c* axis. The J_1 and J_2 potential interaction paths correspond to the dimer bond and the dashed black line, respectively.

Field-Induced Phase Evolution

The magnetization curves below T_N of $BaNd_2ZnS_5$ show kinks around 1.7 T for fields along the [1 -1 0] direction, as shown by Figure 2*a*, indicating a metamagnetic transition. To investigate this transition, single crystal neutron diffraction measurements were performed with an applied magnetic field of 2 and 6 T parallel to the [1 -1 0] direction. As the field-induced transition emerges around 1.7 T, at 1.4 K, the field-dependent magnetic scattering at (1.5 1.5 1) disappears at 1.7 T (see Figure 2*c*) signifying the stripe phase with $\mathbf{q_2}$ = (-½, ½, 0) is no longer present. Therefore, the kink shown in the magnetization measurement is a signature of magnetic order-disorder transition and the corresponding field can be viewed as the critical field H_C for this transition. For the other magnetic sublattice, the magnetic peak (½ ½ 4) gradually decreases with the field increasing but the majority of magnetic peak signal maintains up to 6 T (see Figure 2*c* inset). By analyzing the neutron diffraction data collected 2 and 6 T, the refined magnetic moments for the stripe phase of the $\mathbf{q_2}$ magnetic sublattice with spins along [1 1 0], perpendicular to the field direction, were determined to be 2.8(1) and 2.6(1) μ_B, respectively.

At 2 and 6 T the observed magnetic reflections from the diffraction pattern could be all indexed by $\mathbf{q_1}$= (½, ½, 0), while no peaks could be indexed with $\mathbf{q_2}$= (-½, ½, 0) when considering the body centering translation symmetry. Note, the body-centered unit cell is not a primitive cell and so $\mathbf{q_1}$ and $\mathbf{q_2}$ are not equivalent. From the k-SUBGROUPSMAG program, the low symmetry space group *P*1 (#1.1) was initially selected to test the potential magnetic models. The resulting refinement reveals a partially disordered, liquid-like state of ferromagnetic dimers at 2 T where only the AFM order of the magnetic sublattice with moments along [1 1 0] ($\mathbf{q_1}$ magnetic sublattice) survives indicating the two magnetic sublattices become decoupled under an applied field, as

shown by the magnetic structure in Figure 2*e*. The results also indicate that the interactions between the two magnetic sublattices are weak, i.e., no strong asymmetric interactions between the orthogonally arranged neighboring Nd spin dimers. Considering the magnetic interaction distance and the localized *f*-electron feature for the rare-earth spins, both J_2 and J_z are likely weak comparing to the intra-dimer interaction J_1. Therefore, the SSL in $BaNd_2ZnS_5$ can be viewed as two nearly decoupled square lattices of ferromagnetic dimers that are loosely 3-dimensionally connected. While the magnetic phase transitions induced by the field up to 9 T along [1 -1 0] is likely only within the $\mathbf{q}_2$ magnetic sublattice with Nd moments along [1 -1 0]. Therefore, the following discussions will be focused on only the magnetic dimer square sublattice with spins parallel to the field [1 -1 0].

Neutron diffraction revealed that the $\mathbf{q}_2$ stripe order is fully suppressed by the field at the critical field $H_C \sim 1.7$ T. Field-induced magnetic signal on top of the nuclear Bragg peaks were refined as uniformly aligned moments of 1.2(2) μ_B at 2 T for the magnetic sublattice with the spin Ising axis along [1 -1 0] // **H**, i.e., 0.6(1) μ_B per Nd if averaging it for the whole magnetic lattice, consistent with the increased magnetization in the bulk measurement. If we consider the model of square lattice of ferromagnetic dimers as described above, each ferromagnetic dimer includes two parallel aligned spin-half moments and so makes a spin-1 dimer with S = 1. When a field is applied, two kinds of dimer spin transitions among three magnetic components (S_Z = -1, 0, +1) can occur and cause the order-disorder transition and yield the average induced moment seen by neutrons. One is a spin-flip transition from S_Z = -1 to S_Z = +1 and the other one is a spin-flop transition from S_Z = -1 to S_Z = 0, quantum version of the well-known spin-flop transition in a weak-magnetic-anisotropic AFM system .[46,47] The both spin component transitions are illustrated in Figure 3*b*. The flipped or flopped spin dimers are disordered in lattice space because no additional superlattice

ordering peaks were observed. Here we cannot conclude whether a short-rang order or an only local-correlated dimer spin liquid state exists at H_C with our current diffraction data. Therefore we refer this partial disorder as a liquid-like state. At lower temperatures, the liquid state of ferromagnetic dimers could stay, similar to that happens for Luttinger liquid state in the SSL material Yb_2Pt_2Pb[40] and the quantum spin liquid phase in the Kitaev honeycomb-lattice $RuCl_3$[48], or transit to magnetization plateau phases when thermal and quantum fluctuations are reduced, similar to that reported as "spin-ice" states in the kagome material HoAgGe[49]. At 6 T the square magnetic sublattice with Nd spins along [1 -1 0] enters a field polarized state and has a refined magnetic moment of 2.8(1) μ_B, the magnetic structure is shown in Figure 2*f*.

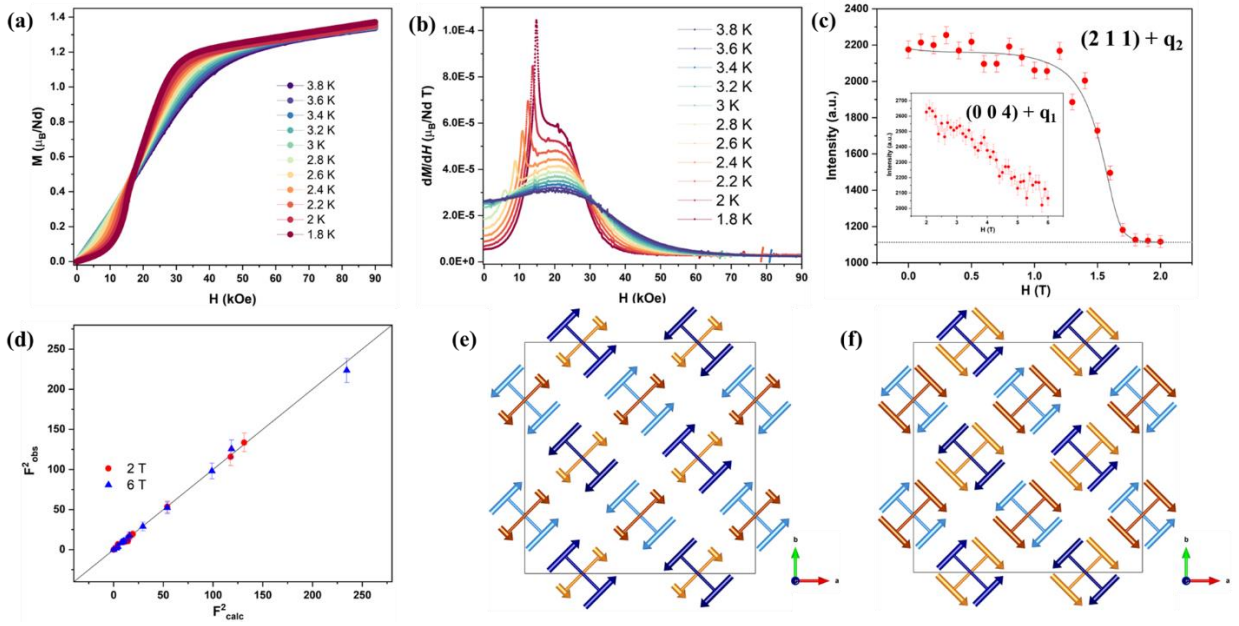

Figure 2. a Magnetization measurement with **H**//(1-10) from 1.8 – 3.8 K. **b** Plots of d*M*/d*H* measured at constant temperature from 1.8-3.8 K, data was smoothed for the derivation. **c** Field-dependent order parameter from 0-2 T at (1.5 1.5 1). The inset for the field-dependent order parameter from 2-6 T at (½ ½ 4). **d** Experimental versus calculated structure factors at 2 T (red circles) and 6 T (blue triangles). **e** The refined magnetic structure of the partially disordered phase at 2 T and **f** the field polarized state at 6 T.

Phase Diagram and Spin Dimer Liquid

We can construct the field-temperature (*H*-*T*) phase diagram from the magnetization data upon varying temperature since neutron diffraction reveals that the kink observed in the magnetization indicates the disorder transition from the stripe order in the $\mathbf{q}_2$ magnetic lattice. The critical field H_C at each temperature can be better observed as a sharp peak in the plots of d*M*/d*H* (see Figure 2*b*), where upon cooling the temperature the H_C shifts towards higher fields, H_C ~1.5 T at 1.8 K. Above H_C, the transition to the field polarized state can be seen by the broad bump feature at higher field. A contour plot mapping the values of d*M*/d*H* obtained from 1.8 – 3.8 K, is depicted in a *H* versus *T* (*H*-*T*) phase diagram describing the magnetic sublattice with spins parallel to the field direction [1 -1 0], Figure 3*a*, based on the bulk magnetization (circles) and susceptibility (diamonds and triangles) measurements under the field along [1 -1 0] and neutron data (square). Phase I represents the 2-**Q** magnetically ordered stripe phase while phase II is the partially disordered, liquid-like state of ferromagnetic dimers, where the magnetic structure determined at 2 T at 1.4 K is shown in Figure 3*a* in the phase II region. The contour plot of d*M*/d*H* clearly defines the regions for Phase I and II and furthermore the transition to the field polarized state as Phase III. According to neutron diffraction measurement at 1.4 K, no additional magnetic order was observed when the stripe phase enters the spin dimer liquid state, Phase II, at 1.7 T, indicating the critical region is further narrowed towards a possible critical point.

A similar temperature dependence of the behavior of H_C in Figurer 3*a* has been observed in the phase diagrams of geometrically frustrated lattices exhibiting field-induced quantum criticality, such as $CoNb_2O_6$ [50,51] and $RuCl_3$ [48], constructed from heat capacity measurements under the field. A possible explanation of such a *H*-*T* behavior in $BaNd_2ZnS_5$ can be explained by field-melting the stripe ordered phase through “spin-flip-or-flop transitions. The *H*-*T* phase diagram

could also suggest the possibility that quantum criticality may exist in $BaNd_2ZnS_5$ at the lowest temperature. To explore these scenarios and reveal the enigmatic magnetic ground state of $BaNd_2ZnS_5$, low temperature heat capacity, magnetization and inelastic neutron scattering measurements are required.

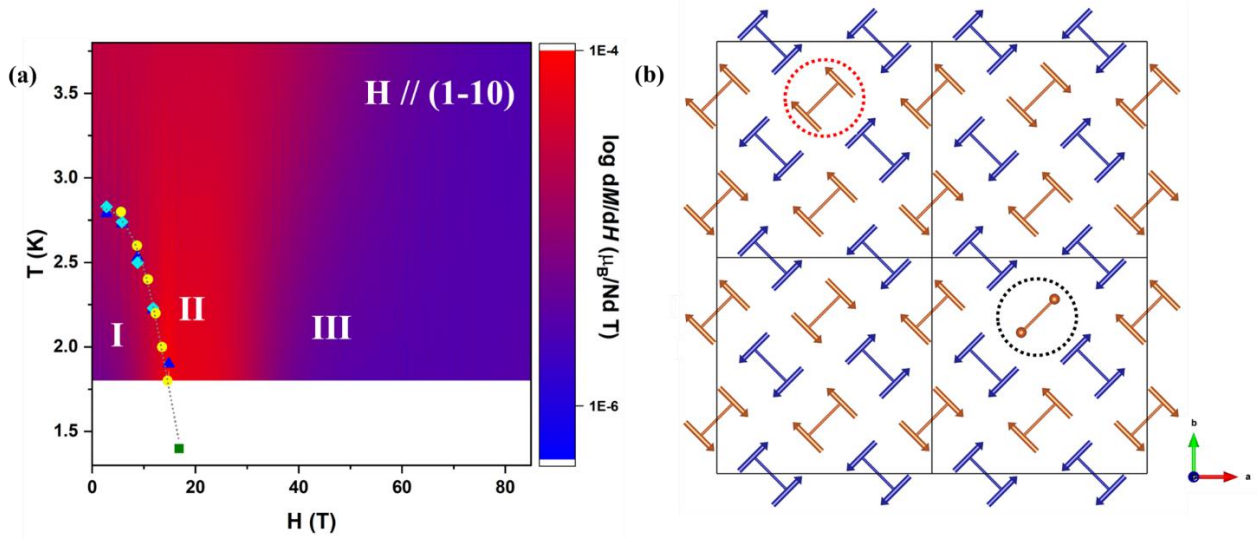

Figure 3. a Field versus T_N (H-T) phase diagram with **H**//(1-10), the magnetic susceptibility, magnetization and neutron data are represented by the light blue diamonds and blue triangles for the two measurements which were performed, yellow circles and green squares, respectively. The H-T phase diagram overlays a contour plot mapping the values of dM/dH obtained at constant temperatures, the values of dM/dH are represented by the color scale. **b** A possible dynamical magnetic pattern at the H_C, the red-circle highlights the spin-flip transition from S_Z = -1 to S_Z = +1 and the black-circle highlights the spin-flop transition from S_Z = -1 to S_Z = 0, the orange circles symbolize no magnetic moment is present.

Summary

Single crystals of $BaNd_2ZnS_5$ from the BaR_2ZnS_5 family have been successfully synthesized and studied by magnetic bulk measurement and neutron diffraction under magnetic

field. Ising magnetic anisotropy of the Nd spins is revealed by the local magnetic susceptibility method with polarized neutrons and their Ising directions are orthogonal to the dimer bonds. Such an arrangement of Ising spins implies no symmetric interactions between the orthogonally arranged dimers. The zero-field magnetic order is a 2-**Q** AFM order of FM dimers with Nd spins along their local Ising directions. Two magnetic sublattices with $\mathbf{q_1}$= (½, ½, 0) and $\mathbf{q_2}$= (-½, ½, 0) constitute the 2-**Q** structure and respond to the field along [1 -1 0] differently. The $\mathbf{q_2}$ magnetic order is suppressed at a critical field, responsible for the kink observed in the magnetization measurement. While the $\mathbf{q_1}$ magnetic sublattice stays mostly unchanged until 6 T. According to this information, we built the *H-T* phase diagram from the bulk magnetization and magnetic susceptibility. A critical region was manifested as a spin dimer liquid phase growing out between the stripe phase at lower field and the field polarized phase at upper field. "Spin-flip" and "spin-flop" mechanisms were proposed to explain the formation of liquid state. Whether the liquid phase of ferromagnetic dimers could condense at an ultra-low temperature deserves further study. As $BaNd_2ZnS_5$ exhibits a unique 2-**Q** magnetic square lattice with weak interactions between orthogonal dimers, it can be an exciting candidate to exhibit unique high order symmetries and a potential host for exotic quantum phases. Future dynamic studies including inelastic neutron scattering can provide insight into magnetic interactions and emergent states in the $BaNd_2ZnS_5$ SSL and discover interesting dynamic properties of ferromagnetic dimers. An effort in synthesizing large, high quality single crystals is thus called for, as available high-quality single crystals make all these possible.

Methods

Neutron Diffraction

To determine the magnetic order single crystal neutron diffraction experiments on the HB-3A DEMAND[52] at the High Flux Isotope Reactor at Oak Ridge National Laboratory. A 1.5 mm sample was measured with the two-axis mode down to 1.4 K using a cryomagnet and a wavelength of 1.542 Å from a bent Si-220 monochromator[53]. The measurement was performed with an applied magnetic field of 0, 2 and 6 T parallel to [1 -1 0]. The Bilbao Crystallography Server[54] was used for the magnetic symmetry analysis and Fullprof software[55] for the magnetic structure refinement. Polarized single crystal neutron diffraction measurements was likewise performed on the HB-3A DEMAND with a polarized neutron beam of 1.542 Å and the calibrated neutron polarization is 72%. The crystal was loaded in a closed-cycle refrigerator with a permanent magnet set providing the fixed field of 0.5 T along [1 -1 0]. We measured 17 flipping ratios at 4 K, above T_N. To analyze the resulting flipping ratios the Cryspy[56] software was used.

References

1. Balents, L. Spin liquids in frustrated magnets. *Nature* **464**, 199–208 (2010).
2. *Introduction to Frustrated Magnetism*.
3. Smith, R. W. & Keszler, D. A. Synthesis, structure, and properties of the orthoborate SrCu2(BO3)2. *Journal of Solid State Chemistry* **93**, 430–435 (1991).
4. McClarty, P. A. *et al.* Topological triplon modes and bound states in a Shastry–Sutherland magnet. *Nature Phys* **13**, 736–741 (2017).
5. Yang, J., Sandvik, A. W. & Wang, L. Quantum criticality and spin liquid phase in the Shastry-Sutherland model. *Phys. Rev. B* **105**, L060409 (2022).
6. Dwivedi, V., Hickey, C., Eschmann, T. & Trebst, S. Majorana corner modes in a second-order Kitaev spin liquid. *Phys. Rev. B* **98**, 054432 (2018).
7. Eschmann, T., Dwivedi, V., Legg, H. F., Hickey, C. & Trebst, S. Partial flux ordering and thermal Majorana metals in higher-order spin liquids. *Phys. Rev. Research* **2**, 043159 (2020).
8. King, A. D., Nisoli, C., Dahl, E. D., Poulin-Lamarre, G. & Lopez-Bezanilla, A. Qubit spin ice. *Science* **373**, 576–580 (2021).
9. Sriram Shastry, B. & Sutherland, B. Exact ground state of a quantum mechanical antiferromagnet. *Physica B+C* **108**, 1069–1070 (1981).
10. Guo, J. *et al.* Quantum Phases of SrCu2(BO3)2 from High-Pressure Thermodynamics. *Phys. Rev. Lett.* **124**, 206602 (2020).
11. Corboz, P. & Mila, F. Tensor network study of the Shastry-Sutherland model in zero magnetic field. *Phys. Rev. B* **87**, 115144 (2013).
12. Miyahara, S. & Ueda, K. Superstructures at magnetization plateaus in SrCu2(BO3)2. *Phys. Rev. B* **61**, 3417–3424 (2000).
13. Kodama, K. *et al.* Magnetic Superstructure in the Two-Dimensional Quantum Antiferromagnet SrCu2(BO3)2. *Science* **298**, 395–399 (2002).

14. Takigawa, M. *et al.* Incomplete Devil's Staircase in the Magnetization Curve of SrCu2(BO3)2. *Phys. Rev. Lett.* **110**, 067210 (2013).
15. Jaime, M. *et al.* Magnetostriction and magnetic texture to 100.75 Tesla in frustrated SrCu2(BO3)2. *Proceedings of the National Academy of Sciences* **109**, 12404–12407 (2012).
16. Sebastian, S. E. *et al.* Fractalization drives crystalline states in a frustrated spin system. *Proceedings of the National Academy of Sciences* **105**, 20157–20160 (2008).
17. Matsuda, Y. *et al.* Magnetization of SrCu2(BO3)2 in ultrahigh magnetic fields up to 118 T. *Physical review letters* (2013) doi:10.1103/PhysRevLett.111.137204.
18. Kageyama, H. *et al.* Exact Dimer Ground State and Quantized Magnetization Plateaus in the Two-Dimensional Spin System SrCu2(BO3)2. *Phys. Rev. Lett.* **82**, 3168–3171 (1999).
19. Kodama, K. *et al.* Field-induced effects of anisotropic magnetic interactions in SrCu2(BO3)2. *J. Phys.: Condens. Matter* **17**, L61–L68 (2005).
20. Zayed, M. E. *et al.* 4-spin plaquette singlet state in the Shastry–Sutherland compound SrCu2(BO3)2. *Nature Phys* **13**, 962–966 (2017).
21. Koga, A. & Kawakami, N. Quantum Phase Transitions in the Shastry-Sutherland Model for SrCu2(BO3)2. *Phys. Rev. Lett.* **84**, 4461–4464 (2000).
22. Berrada, A. *et al.* Synthese, cristallogenese, proprietes magnetiques et effets magnetostrictifs spontanes de quelques tetraborures de terres rares. *Materials Research Bulletin* **11**, 1519–1526 (1976).
23. Siemensmeyer, K. *et al.* Fractional Magnetization Plateaus and Magnetic Order in the Shastry-Sutherland Magnet ${\mathrm{TmB}}_{4}$. *Phys. Rev. Lett.* **101**, 177201 (2008).
24. Ye, L., Suzuki, T. & Checkelsky, J. G. Electronic transport on the Shastry-Sutherland lattice in Ising-type rare-earth tetraborides. *Phys. Rev. B* **95**, 174405 (2017).
25. Ishii, Y. *et al.* Magnetic properties of the Shastry-Sutherland lattice material BaNd2ZnO5. *Phys. Rev. Materials* **5**, 064418 (2021).

26. Kaduk, J. A., Wong-Ng, W., Greenwood, W., Dillingham, J. & Toby, B. H. Crystal Structures and Reference Powder Patterns of BaR2ZnO5 (R=La, Nd, Sm, Eu, Gd, Dy, Ho, Y, Er, and Tm). *NIST* **104 No. 2**, (1999).
27. Taniguchi, T. *et al.* Antiferromagnetism of R2BaPdO5 (R = La, Nd, Pr, Sm, Eu, Gd, Dy, Ho). *Journal of Alloys and Compounds* **386**, 63–69 (2005).
28. Ishii, Y. *et al.* High-pressure synthesis, crystal structure, and magnetic properties of the Shastry-Sutherland-lattice oxides BaLn2ZnO5 (Ln = Pr, Sm, Eu). *Journal of Solid State Chemistry* **289**, 121489 (2020).
29. Zaremba, V. I., Kaczorowski, D., Nychyporuk, G. P., Rodewald, U. Ch. & Pöttgen, R. Structure and physical properties of RE2Ge2In (RE = La, Ce, Pr, Nd). *Solid State Sciences* **6**, 1301–1306 (2004).
30. Tobash, P. H. *et al.* Crystal Growth, Structural, and Property Studies on a Family of Ternary Rare-Earth Phases RE2InGe2 (RE = Sm, Gd, Tb, Dy, Ho, Yb). *Chem. Mater.* **17**, 5567–5573 (2005).
31. Fischer, P. *et al.* Antiferromagnetic rare-earth ordering in the intermetallic compounds R2Pd2In (R = Pr, Nd). *J. Phys.: Condens. Matter* **12**, 7089–7098 (2000).
32. Miiller, W. *et al.* Magnetic structure of ${\mathrm{Yb}}_{2}{\mathrm{Pt}}_{2}\mathrm{Pb}$: Ising moments on the Shastry-Sutherland lattice. *Phys. Rev. B* **93**, 104419 (2016).
33. Isaev, L., Ortiz, G. & Dukelsky, J. Local Physics of Magnetization Plateaux in the Shastry-Sutherland Model. *Phys. Rev. Lett.* **103**, 177201 (2009).
34. Orendáč, M. *et al.* Ground state and stability of the fractional plateau phase in metallic Shastry–Sutherland system TmB4. *Sci Rep* **11**, 6835 (2021).
35. Wierschem, K. *et al.* Origin of modulated phases and magnetic hysteresis in ${\mathrm{TmB}}_{4}$. *Phys. Rev. B* **92**, 214433 (2015).
36. Iwakawa, K. *et al.* Multiple Metamagnetic Transitions in Antiferromagnet Yb2Pt2Pb with the Shastry–Sutherland Lattice. *J. Phys. Soc. Jpn.* **81**, SB058 (2012).

37. Shimura, Y., Sakakibara, T., Iwakawa, K., Ōnuki, Y. & Sugiyama, K. Magnetization steps in Yb2Pt2Pb with the Shastry-Sutherland lattice. *Journal of the Korean Physical Society* **63**, 551–554 (2013).

38. Ochiai, A. *et al.* Field-Induced Partially Disordered State in Yb2Pt2Pb. *J. Phys. Soc. Jpn.* **80**, 123705 (2011).

39. Kim, M. S. & Aronson, M. C. Spin Liquids and Antiferromagnetic Order in the Shastry-Sutherland-Lattice Compound Yb2Pt2Pb. *Phys. Rev. Lett.* **110**, 017201 (2013).

40. Gannon, W. J. *et al.* Spinon confinement and a sharp longitudinal mode in Yb2Pt2Pb in magnetic fields. *Nat Commun* **10**, 1123 (2019).

41. Michimura, S., Shigekawa, A., Iga, F., Takabatake, T. & Ohoyama, K. Complex Magnetic Structures of a Shastry–Sutherland Lattice TmB4 Studied by Powder Neutron Diffraction Analysis. *J. Phys. Soc. Jpn.* **78**, 024707 (2009).

42. Wakeshima, M. *et al.* Specific heat and neutron diffraction study on quaternary sulfides BaNd2CoS5 and BaNd2ZnS5. *Journal of Solid State Chemistry* **174**, 159–164 (2003).

43. Cao, H. *et al.* Ising versus XY Anisotropy in Frustrated ${R}_{2}{\mathrm{Ti}}_{2}{\mathbf{O}}_{7}$ Compounds as ``Seen'' by Polarized Neutrons. *Phys. Rev. Lett.* **103**, 056402 (2009).

44. Cao, H. B., Gukasov, A., Mirebeau, I. & Bonville, P. Anisotropic exchange in frustrated pyrochlore Yb2Ti2O7. *J. Phys.: Condens. Matter* **21**, 492202 (2009).

45. Billingsley, B. R., Marshall, M., Shu, Z., Cao, H. & Kong, T. Single crystal synthesis and magnetic properties of a Shastry-Sutherland lattice compound BaNd2ZnS5. Preprint at https://doi.org/10.48550/arXiv.2208.12180 (2022).

46. Fiebig, M., Fröhlich, D. & Thiele, H.-J. Determination of spin direction in the spin-flop phase of Cr2O3. *Phys. Rev. B* **54**, R12681–R12684 (1996).

47. Ding, L. *et al.* Noncollinear magnetic structure and magnetoelectric coupling in buckled honeycomb ${\mathrm{Co}}_{4}{\mathrm{Nb}}_{2}{\mathrm{O}}_{9}$: A single-crystal neutron diffraction study. *Phys. Rev. B* **102**, 174443 (2020).
48. Wolter, A. U. B. *et al.* Field-induced quantum criticality in the Kitaev system alpha-RuCl3. *Phys. Rev. B* **96**, 041405 (2017).
49. Zhao, K. *et al.* Realization of the kagome spin ice state in a frustrated intermetallic compound. *Science* **367**, 1218–1223 (2020).
50. Liang, T. *et al.* Heat capacity peak at the quantum critical point of the transverse Ising magnet CoNb2O6. *Nat Commun* **6**, 7611 (2015).
51. Kinross, A. W. *et al.* Evolution of Quantum Fluctuations Near the Quantum Critical Point of the Transverse Field Ising Chain System CoNb2O6. *Phys. Rev. X* **4**, 031008 (2014).
52. Cao, H. *et al.* DEMAND, a Dimensional Extreme Magnetic Neutron Diffractometer at the High Flux Isotope Reactor. *Crystals* **9**, 5 (2019).
53. Chakoumakos, B. C. *et al.* Four-circle single-crystal neutron diffractometer at the High Flux Isotope Reactor. *J Appl Cryst* **44**, 655–658 (2011).
54. Perez-Mato, J. M. *et al.* Symmetry-Based Computational Tools for Magnetic Crystallography. *Annual Review of Materials Research* **45**, 217–248 (2015).
55. Rodríguez-Carvajal, J. Recent advances in magnetic structure determination by neutron powder diffraction. *Physica B: Condensed Matter* **192**, 55–69 (1993).
56. Yamashita, T. *et al.* CrySPY: a crystal structure prediction tool accelerated by machine learning. *Science and Technology of Advanced Materials: Methods* **1**, 87–97 (2021).

Acknowledgements

The research at Oak Ridge National Laboratory (ORNL) was supported by the U.S. Department of Energy (DOE), Office of Science, Office of Basic Energy Sciences, Early Career Research Program Award KC0402020, under Contract DE-AC05-00OR22725. This research used resources at the High Flux Isotope Reactor, a DOE Office of Science User Facility operated by ORNL.

Author Information

Authors and Affiliations

Neutron Scattering Division, Oak Ridge National Laboratory, Oak Ridge, Tennessee 37831, USA

Madalynn Marshall, Xiaojian Bai, Qianli Ma, Huibo Cao

Department of Physics, University of Arizona, Tucson, Arizona, 85721

Brianna R. Billingsley, Tai Kong

Department of Chemistry and Biochemistry, University of Arizona, Tucson, Arizona, 85721

Tai Kong

Contributions

H.C. cultivated the research; B.R.B and T.K. synthesized single-crystal samples and performed magnetization measurements; M.M. and H.C. performed neutron scattering experiments and analyze the data; X.B. assisted with polarized neutron data analysis; X.B. and Q.M. contributed to theoretical discussion; M.M. and H.C. wrote manuscript with comments from all authors.

Corresponding Author

Correspondence to Dr. H. Cao (caoh@ornl.gov).